Pellet Printing for Soft Devices

*Yijia Wu, Ju-Hung Chen, Ariana Olivares, Katherine Kostak, Stefan Pedicone, Savita V. Kendre, and Markus P. Nemitz**

Y. Wu, J. Chen, A. Olivares, K. Kostak, S. Pedicone, Dr. S. Kendre, Prof. M. P. Nemitz

Department of Mechanical Engineering, Tufts University, Medford, MA 02155, USA

Email Address: markus.nemitz@tufts.edu

Keywords: *fused granulate fabrication, airtight additive manufacturing, 3D printing, thermoplastic elastomers, soft robots*

Rapid prototyping of soft devices is often limited by manual fabrication and additive manufacturing methods that are costly, material-restricted, or require extensive post-processing. Fused Granulate Fabrication (FGF) offers a rapid, scalable alternative by extruding thermoplastic pellets through a screw-based extruder directly onto the build surface, enabling continuous, high-throughput printing. It also supports a broad range of materials, from rigid plastics to silicone-soft elastomers (Shore 6A). Reliable printing of airtight pneumatic soft structures with a volumetric flow rate up to 5 mm^3/s was achieved by addressing the root causes of inconsistent extrusion and stringing through integrated hardware, material, and parameter optimizations. Mechanical performance of thermoplastic styrenic block copolymer pellets was characterized, revealing good elastic recovery and Mullins-effect-induced softening. Fatigue testing of FGF-printed pneumatic actuators demonstrated durability over 100,000 bending cycles, and behavior was cross-validated with numerical simulations using Ogden hyperelastic models. Demonstrated applications include a pneumatically actuated robotic hand with 15 segments, a multi-chamber robotic fish with an articulated fin, and a soft pressure cuff for blood pressure monitoring. FGF enables the fabrication of airtight, functional soft devices using commercially available thermoplastic pellets, offering a versatile, cost-effective, and scalable alternative to traditional soft device manufacturing methods.

1 Introduction

Soft robotics is a transformative field that enables the creation of highly adaptable, compliant, and biomimetic systems [1], with applications spanning medical devices [2], assistive wearables [3], robotic locomotion [4], and manipulation [5], among others. The intrinsic deformability of soft materials enhances safety in human-robot interaction, improves resilience to mechanical impact, and, in some cases, simplifies fabrication [4], thereby enabling functionalities beyond the reach of traditional rigid-bodied robots. Nonetheless, the fabrication of soft systems, particularly those requiring airtight architectures and soft materials in the Shore 00 scale, remains a major challenge. Soft lithography using additive-curing elastomers can yield such material properties but involves labor-intensive workflows, limited scalability, and a strong dependence on operator skill, which constrains reproducibility and broader dissemination beyond specialized laboratories [6]. State-of-the-art demonstrations, including multi-gait soft robots [4], bistable valves [7], and soft grippers [8], often depend on custom molds, manual assembly, and extensive post-processing.

Digital fabrication techniques, including Fused Filament Fabrication (FFF), Direct Ink Writing (DIW), Stereolithography (SLA), Material Jetting (MJ), and Selective Laser Sintering (SLS) have been explored as mold-free approaches for fabricating soft robotic systems. However, each method exhibits specific limitations that have hindered widespread adoption, with soft lithography remaining the dominant fabrication approach for soft robots [9, 10, 11]. FFF is widely used for its affordability and accessibility, but it is limited by the material properties of available filaments. Most soft filaments are thermoplastic polyurethanes (TPU) with Shore hardness 60A or higher, which are prone to buckling or jamming in the extruder, leading to unreliable fabrication of soft components [12]. DIW enables the extrusion of custom-formulated inks [13], including silicones [14] and hydrogels [15]. Although capable of printing soft materials in the Shore 00 scale, DIW is limited by slow print speeds, time dependent curing processes, limited tolerances for overhang, and the need for extensive ink formulation, rheological tuning, and post-processing [9]. These challenges have hindered the broader adoption of DIW in soft robotics. SLA and MJ systems offer higher print resolution than FFF and DIW. However, both SLA and MJ require post-processing, are maintenance-intensive, and use photopolymers. Commercially available soft photopolymers are typically brittle and exhibit viscoelastic behavior, characterized by material hysteresis that introduces time-dependent delays between applied force and resulting displacement [10]. Photopolymers are also susceptible to long-term degradation under UV exposure [16, 17]. The cyclic fatigue performance of MJ-printed actuators is constrained by the intrinsic material properties of photopolymers, which fail after fewer cycles com-

pared to thermoplastic-based actuators under equivalent loading conditions [18, 19]. Although MJ enables multi-material printing, interfacial degradation between dissimilar materials remains a limiting factor, with failures commonly observed after only thousands of cycles [20]. SLS eliminates the need for support structures, as the unsintered powder naturally supports the part during printing, but also raises great challenges in powder removal for parts with complicated internal channels. It is also limited in elastomeric material options with Shore hardness 40A and above.

Given the accessibility and low cost of FFF, there is growing interest in layer-by-layer thermoplastic deposition for the fabrication of soft devices, ranging from pneumatic actuators [21, 22, 23, 24, 25], to multi-material printed sensors [26], pneumatic logic devices [27, 7], and fully integrated print-in-place robots with embedded sensing and control [7, 8, 28]. Several strategies have been developed to improve the air-tightness of prints using FFF, including printing in an inverted orientation to promote gravity-assisted layer sealing and reduce interfacial voids [28]; optimizing G-code using Euler paths to minimize start-stop artifacts and improve extrusion continuity [8]; and implementing vision-based closed-loop control to detect and correct defects in real time during the printing process [12]. While promising, FFF is limited to printing relatively stiff elastomers compared to silicones and remains constrained by inherently low volumetric flow rates imposed by its filament-based feeding mechanism. Fused Granulate Fabrication (FGF) similarly deposits thermoplastics layer by layer, but instead of relying on filament feedstock, it directly processes raw thermoplastic pellets through a screw-based extruder [29, 30]. This approach allows for a broader selection of thermoplastic elastomers (TPE) that are not available as filaments; for instance, thermoplastic styrenic block copolymers (TPS) can reach lower Shore hardness values than other TPE classes. Despite its potential, FGF remains largely unknown and underexplored in the soft robotics community. Notable exceptions include the work of Georgopoulou et al., who developed custom conductive Styrene-Ethylene-Butylene-Styrene (SEBS) pellets to fabricate sensorized pneumatic actuators using a multi-step printing process [31], and cable-driven fingers enabled by multi-material printing [32]. Khondoker et al. developed a pellet-based printer that feeds molten material from a screw extruder to the print head via a heated hose. However, their demonstration was limited to two materials: a 47A thermoplastic elastomer (Kraton G1657) and a rigid shape memory polymer [33]. Building on this design, Morita et al. integrated a needle valve mechanism into the pellet extrusion system to mitigate stringing during non-deposition travel of the print head [34]. Willemstein et al. explored SEBS pellets with low Shore hardness (as low as 00-30), but printing was restricted to thin membranes due to fabrication constraints [35].

These limited studies on FGF focused on a small subset of materials and missed the opportunity to explore key performance metrics such as elastic recovery, strain softening, and fatigue behavior of soft pellets. As a result, thermoplastic elastomers across the Shore 00 and A hardness scales remain largely uncharacterized. The design space of pellet-based printing also remained underexplored, with few compelling demonstrations of large-scale or mechanically complex soft devices fabricated from elastomeric pellets. Prior efforts have not introduced accessible or standardized hardware platforms to enable broader adoption. Instead, existing systems rely on customized, non-commercial setups with limited assessment of their reliability.

Here, we evaluate FGF for the fabrication of soft devices and systematically characterize the mechanical properties of thermoplastic pellets ranging from Shore hardness 6A (00-55) to Shore hardness 50A (00-85). We assess device performance by numerically modeling and experimentally testing pneumatic actuators of varying Shore hardness, surpassing 100,000 actuation cycles. Compared to FFF, FGF prints up to four times faster, more reliably produces airtight structures, and eliminates oozing through the selection of pellets with high melt viscosities. We demonstrate its applicability through functional soft devices, including a pneumatically driven soft hand with 15 individually addressable segments, a multi-chamber robotic fish with an articulated fin, and a pressure cuff for measuring systolic pressure. These results establish FGF as a robust, accessible, and cost-effective digital fabrication strategy for the rapid prototyping of large soft devices (tens of centimeters) using materials with softness comparable to silicones. With hundreds of thousands of thermoplastic pellets commercially available, FGF enables an expansive and previously inaccessible material palette for the fabrication of soft devices with applications in field robotics, medical devices, wearables and beyond.

2 Pellet printing with soft materials

2.1 Operating principle

FGF, also known as pellet printing, operates on the same fundamental principle as FFF, wherein a 3D object is constructed layer by layer through the localized deposition of molten thermoplastic. Unlike FFF, which uses filament as feedstock, FGF employs thermoplastic pellets that are conveyed by gravity or pneumatics into a screw-driven extruder. Inside the heated barrel, a rotating screw transports, mixes, and compresses the pellets, which are subsequently melted by the surrounding heating elements and forced through a heated nozzle to deposit the thermoplastic material (**Figure 1A**). This screw-driven

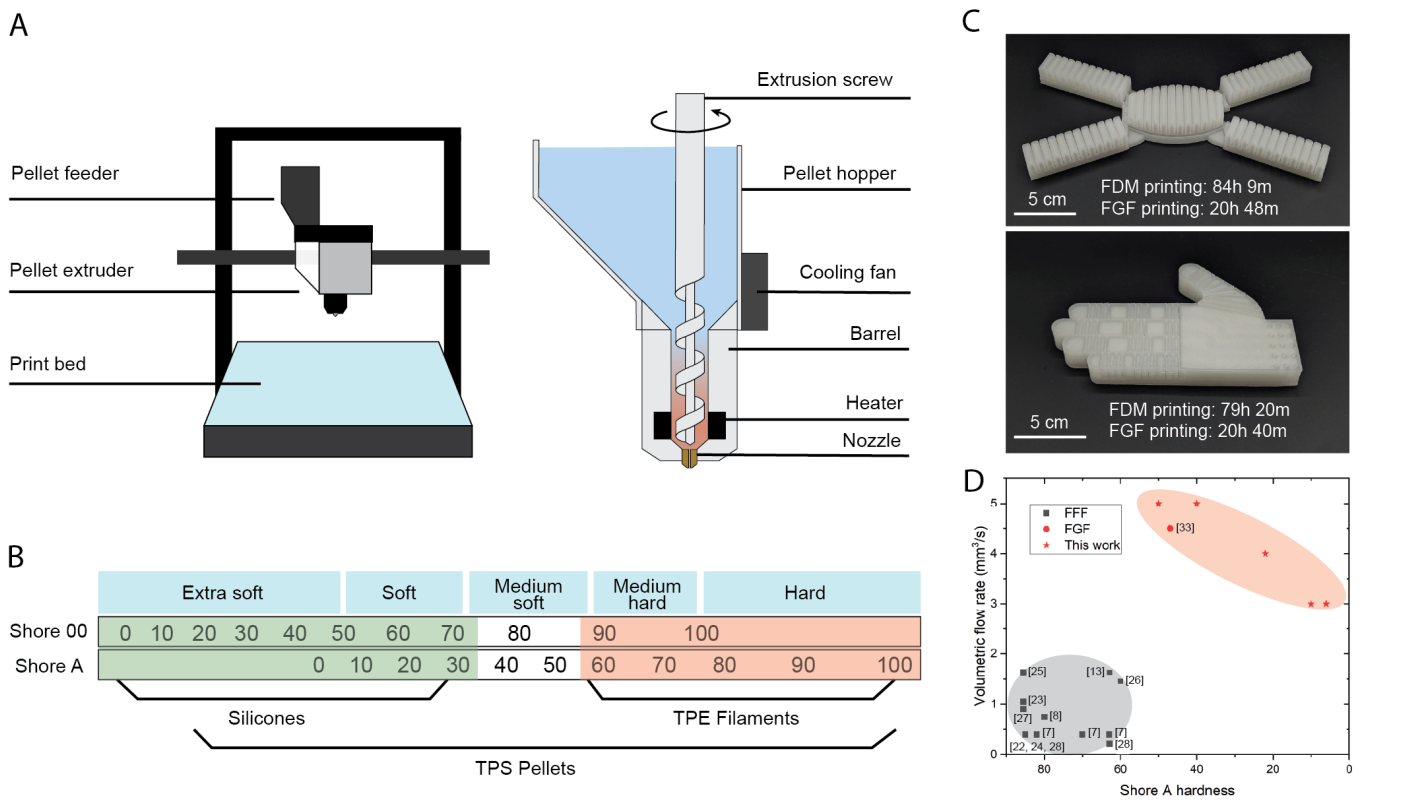

Figure 1: **Overview of the Fused Granulate Fabrication (FGF) printing process.** (A) Schematic of our FGF printer using a screw-based pellet extruder. (B) Comparison of Shore hardnesses across commercially available silicones, TPE filaments, and TPS pellets, illustrating the broader softness range accessible through pellet-based materials. (C) Comparison of printing times between FGF and FDM, demonstrating that FGF significantly accelerates the fabrication of large soft structures, using print parameters in Supporting Information, Table S2. (D) Estimated volumetric flow rate versus Shore A hardness from prior FFF and FGF studies on airtight soft robot fabrication, highlighting that FGF achieves higher volumetric flow rates while supporting softer materials than FDM.

extrusion process supports higher flow rates and a wider range of printable materials compared to filament-fed FFF systems. Filaments are inherently difficult to extrude, as they function like pistons, susceptible to buckling when too soft. In contrast, pellet-fed systems decouple mechanical rigidity from processability, enabling the reliable extrusion of materials with low Young's moduli including those with stiffness levels comparable to silicones (**Figure 1B**). The high extrusion rate of FGF enables the rapid fabrication of large structures that would be prohibitively time-consuming to produce with conventional FFF printers. For instance, printing airtight pneumatic components with FFF typically requires a 0.1 mm layer height and print speeds below 10 mm/s to maintain sealing quality. In contrast, the FGF process presented in this study produces reliable airtight structures using a 0.2 mm layer height at 30 mm/s for 22A TPS pellets, resulting in an increase in print throughput. Even higher speeds are achievable for stiffer material and less complex structures while maintaining airtightness (**Supporting Information, Section 4**). Representative demonstrations include the printing of a pneumatically powered multigait soft robot and soft robotic hand (**Figure 1C**). To quantify this advantage, we analyzed published studies re-

porting airtight soft robotic components fabricated via either FFF or FGF. Volumetric flow rates Q (mm^3/s) were estimated by combining reported nozzle diameters d (mm), layer heights h (mm), and print speeds v (mm/s), using the relation $Q = d \times h \times v$ and assuming extrusion width is equal to nozzle diameter. The resulting plot of volumetric flow rate versus material Shore hardness reveals that FGF consistently achieves higher flow rates, particularly for softer materials (**Figure 1D**).

2.2 Best practices for reliable pellet printing

FGF offers various advantages over FFF, including access to a much wider range of materials, higher volumetric flow rates, and reliability in producing airtight prints. However, it also presents challenges, most notably (i) inconsistent extrusion and (ii) stringing (**Figure 2A**), which are pronounced when printing soft materials with Shore 00 hardness, comparable to silicones.

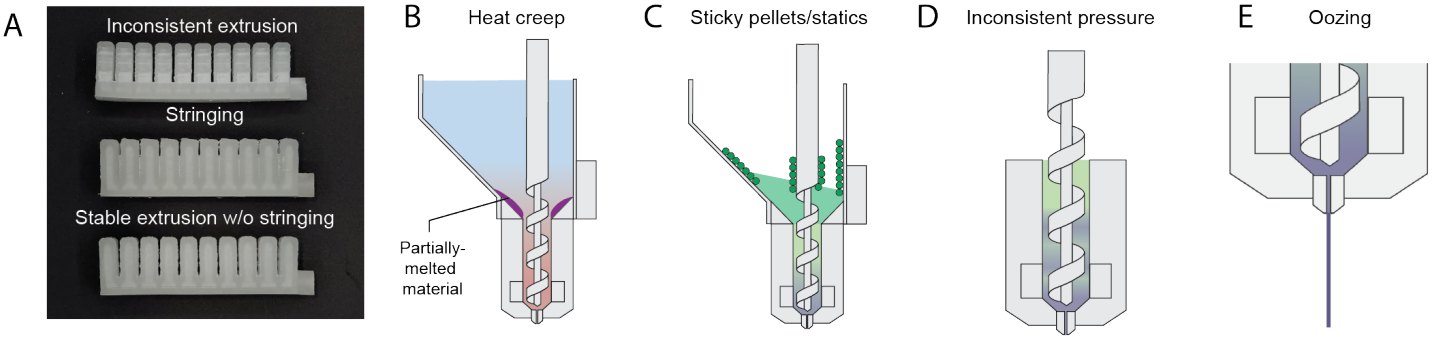

Figure 2: **Challenges towards reliably printing soft airtight structures with FGF.** (A) Images of printed pneumatic actuators highlighting two common defects, inconsistent extrusion and stringing, that can compromise functionality, alongside an optimized print demonstrating successful mitigation through tuning. (B–D) Causes of inconsistent extrusion include: heat creep from inadequate thermal management, poor pellet feed due to adhering pellets, and pressure fluctuations in the barrel caused by improper flow rate. (E) Stringing is caused by continued oozing of molten material from the nozzle after screw rotation ceases, facilitated by the low melt viscosity of the selected print material.

2.2.1 Inconsistent extrusion

Inconsistent extrusion leads to non-uniform wall thickness, which may result in leakage through under-extruded regions or require elevated actuation pressures in over-extruded areas of the printed soft device. Inconsistent extrusion typically results from (i) heat creep (**Figure 2B**), (ii) sticky or statically charged pellets (**Figure 2C**), or (iii) inconsistent pressure within the barrel (**Figure 2D**).

Heat creep occurs when thermal energy from the heated barrel conducts backward along the extruder components, partially melting pellets before they reach the intended melting zone. This premature softening can cause pellets to deform or fuse together, leading to blockages or erratic feeding behavior. After analyzing infrared images from a thermal camera, we installed a high-speed cooling fan at the extruder

to ensure effective thermal control and mitigate heat creep (**Supporting Information, Section 3**). Pellet flow can be disrupted by surface adhesion among pellets. Pellet adhesion arises from the polymer composition, electrostatic charge accumulated during pellet handling and transport, and absorbed moisture. These effects can lead to irregular feeding, bridging, or clogging, as accumulated pellets obstruct the transport of material into the extruder barrel and prevent consistent pellet entry into the melt zone. We addressed accumulation and feeding issues by screening pellets of similar Shore hardness to identify those with inherently low surface adhesion and reduced susceptibility to static charge (**Supporting Information, Section 2**). We also dehumidified the pellets prior to printing to eliminate moisture-induced cohesion. On the hardware side, the pellet hopper was redesigned with a steeper wall angle to enhance gravitational flow, and the internal surfaces were coated using a polytetrafluoroethylene (PTFE) spray to reduce wall friction and mitigate pellet bridging.

After resolving hardware and material issues, we continued to observe intermittent extrusion inconsistencies. We identified the root cause as a mismatch between the commanded and actual extrusion rates. Excess flow or slow print speed caused molten material to accumulate above the nozzle, generating back pressure that led to brief over-extrusion once a threshold was exceeded. Conversely, insufficient flow or high print speed caused under-extrusion. We resolved this issue by fine-tuning the print speed and flow rate and keeping the parameters static throughout the print to maintain a stable extrusion balance (**Supportin Information, Section 5**).

2.2.2 Stringing

Stringing refers to unintended thin strands of thermoplastic forming between printed features due to residual oozing during non-print travel of the print head (**Figure 2E**). Even when the extrusion screw halts, molten material may continue to ooze due to gravity and residual back pressure within the barrel. This effect is particularly pronounced with soft, elastic materials and can result in geometric distortions, internal voids, and ultimately leakage or performance degradation. In FFF systems, stringing is typically mitigated through parameter tuning or filament retraction, though these strategies can introduce extrusion instability when applied to elastomers. FGF offers a distinct advantage by providing access to a broader range of pelletized materials, enabling material selection as an additional strategy for reducing stringing.

In this work, we mitigated stringing by selecting materials with high melt viscosity and optimizing flow rate and extrusion length during slicing to minimize residual oozing (**Supporting Information, Sec-**

tion 2 and 5). Materials with high melt viscosity resist dripping under zero shear conditions while remaining processable under shear during extrusion. By carefully tuning both material selection and process parameters, we established a process window that consistently yielded airtight soft structures with minimal stringing. We also tested modest screw retraction settings to alleviate pressure buildup; however, their effectiveness was limited when using materials with low melt viscosity.

3 Material characterization

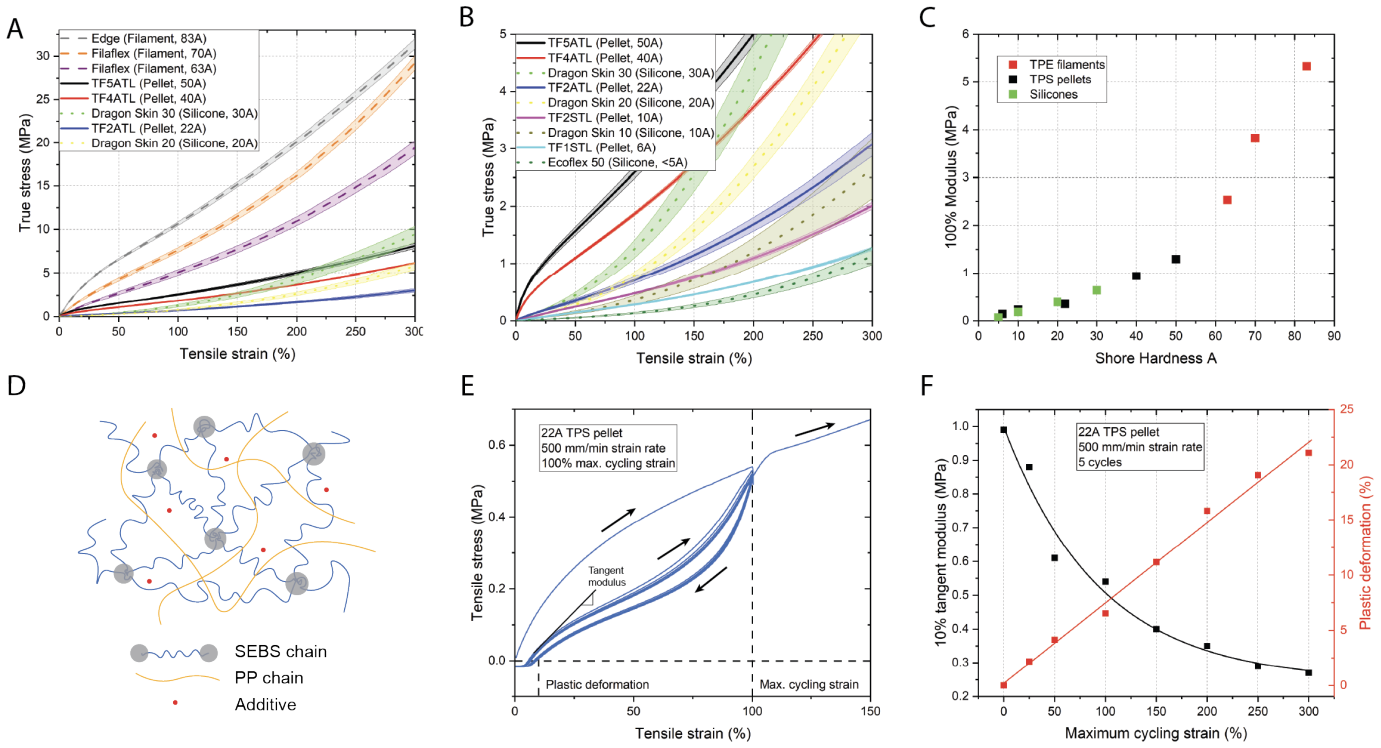

Figure 3: **Mechanical characterization of TPE filaments, TPS pellets, and silicone materials for soft structure fabrication.** (A) True stress–strain curves up to 300% strain, with shaded 95% confidence intervals from five tests. (B) Zoomed-in view highlighting low-modulus behavior in softer materials. (C) 100% tangent modulus versus Shore hardness, showing the stiffness–hardness correlation. (D) Microstructure of a SEBS–PP blend TPS material. PP is always mixed in TPS materials to tune elasticity and processability. (E) Representative tensile cycling test on 22A TPS pellets, illustrating loading–unloading behavior, tangent modulus, and plastic deformation. (F) Effect of maximum cycling strain on 10% tangent modulus and plastic deformation for 22A pellets.

To guide our material selection and better understand the behavior of printed structures, we characterized the mechanical properties of representative TPE filaments, TPS pellets, and silicone rubbers. We prepared five dogbone samples for each material using FDM printing, FGF printing, and molding, following the ASTM D412 standard, and tested them under uniaxial tension. We converted the engineering strain to true strain to more accurately capture nonlinear behavior at low strain. We plotted stress-strain curves up to 300% strain along with 95% confidence intervals for each material (**Figure 3A**). Our

results show that TPE filaments exhibit high stiffness and strain-softening behavior within the first 100% strain, reflecting their high initial modulus and limited stretchability. In contrast, TPS pellets demonstrate significantly lower stiffness. Softer pellets, especially those with Shore hardness below 22A, indicate low modulus and minimal initial softening, exhibiting mechanical behaviors similar to commercial silicones (**Figure 3B**). The observed correlation between the 100% tangent modulus and Shore hardness confirms the general trend of increasing modulus with Shore hardness and highlights the broader modulus range achievable with TPS pellets (**Figure 3C**).

Commercial TPS pellets not only contain SEBS but also Polypropylene (PP) (**Figure 3D**). PP helps with tuning the elasticity and processability of the TPS material, but also leads to a more severe Mullins effect, which is an irreversible stress-softening observed in elastomers after the first loading cycle (**Supporting information, Figure S3A**). To assess elastic recovery and material fatigue, we conducted cyclic tensile tests on 22A TPS pellets at a strain rate of 500 mm/min with incremental strain limits. The loading-unloading curve of 22A pellets highlights the reduction in tangent modulus and the presence of permanent plastic deformation (**Figure 3E**). Most mechanical degradation occurs during the first cycle, with subsequent cycles showing more stable behavior. Increasing the maximum strain leads to a monotonic increase in plastic deformation and decrease in the 10% tangent modulus (**Figure 3F**).

4 Case study: Pellet printed pneumatic actuators

4.1 Mechanical characterization of pellet printed PneuNets

To evaluate the performance of soft devices printed via FGF, we designed a pneumatic actuator (PneuNet), and fabricated and tested it using TPS pellets of varying Shore hardness. We characterized actuation performance by quantifying the bending angle as a function of input pressure (**Figure 4A**) and also compared them with silicone molded and filament printed PneuNets (**Supporting information, Figure S4**).

To assess long-term durability, we subjected the 22A actuator to continuous operation for up to 100,000 actuation cycles (**Figure 4B**). The pressure–bending relationship remained consistent throughout the test, with minimal degradation in peak angle or response behavior. This result confirms that soft actuators fabricated via FGF can maintain airtightness and mechanical integrity over prolonged use. A distinct change between the first and second cycle reflects the Mullins effect, which stabilizes in subsequent cycles and does not compromise functionality over time. The Mullins effect observed in 3D-printed

structures fabricated from TPS pellets can be interpreted as a mechanical programming step, during which the actuator is conditioned prior to reaching its steady-state performance. This stress-softening behavior may be strategically exploited as a functional feature, where the initial inelastic deformation is harnessed to achieve application-specific mechanical responses.

We also investigated the influence of extrusion flow rate on actuator performance (**Figure 4C**). Under-extrusion led to poor layer adhesion and internal leakage, whereas over-extrusion introduced stringing and geometric deformation. By optimizing the extrusion process through flow rate adjustment, we repeatably produced airtight actuators with consistent bending behavior. However, Finite Element Analy-

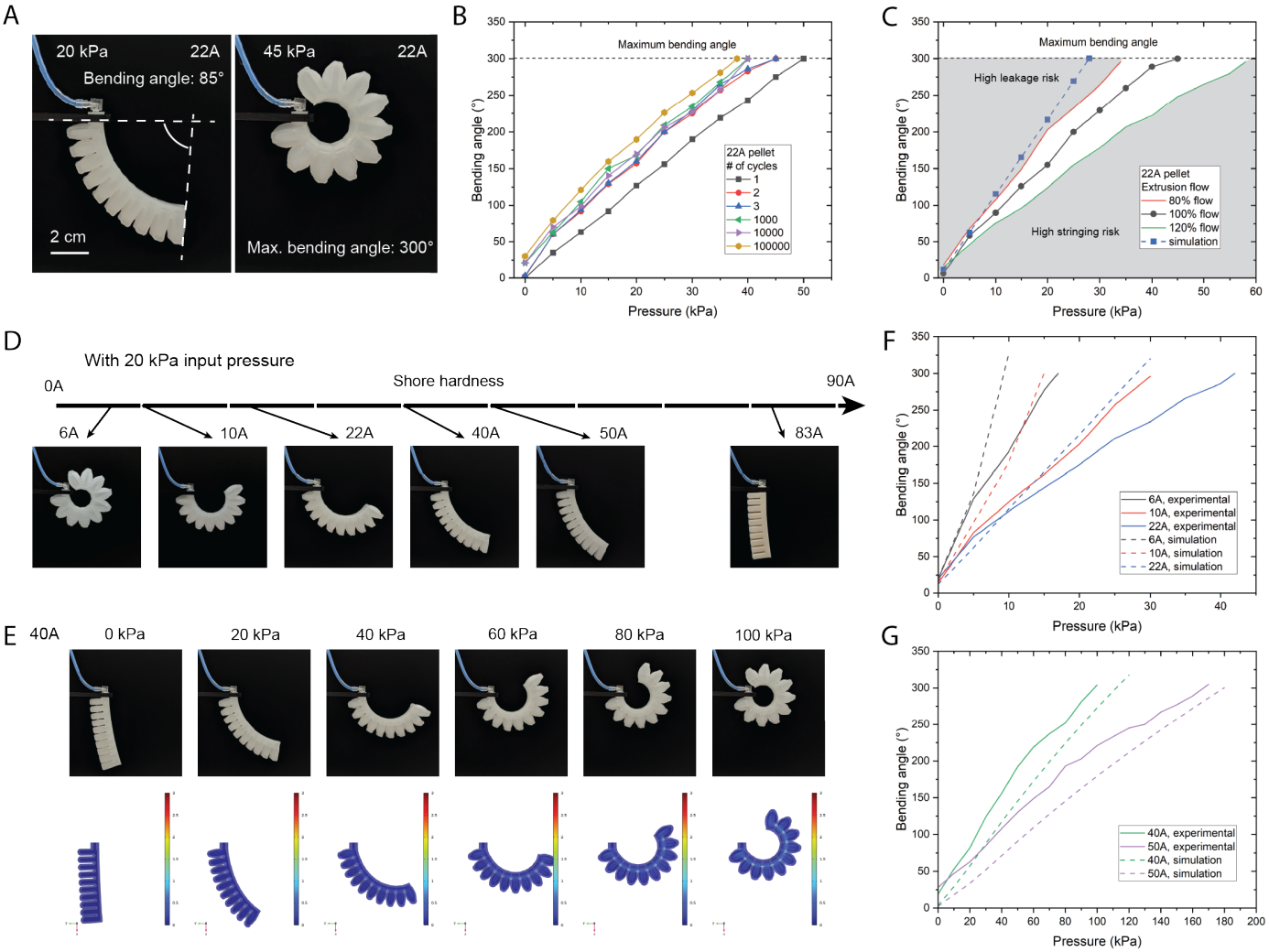

Figure 4: **Characterization of soft actuators printed with TPS pellets using FGF.** (A) PneuNet actuator printed with 22A pellets, showing bending angle measurement and experimentally limited maximum bending. (B) Bending angle versus pressure over 1–100,000 actuation cycles, demonstrating stable performance. (C) Effect of extrusion flow rate on bending behavior; shaded regions indicate leakage and stringing risks. The flow percentage represents the relative setting compared to the recommended flow rate for the 22A pellet and does not correspond to the actual flow rate. (D) Bending comparison of actuators with different Shore hardness at 20 kPa. (E) Experimental vs. simulated deformation of a 40A actuator under increasing pressure. (F) Bending angle versus pressure for 6A, 10A, and 22A actuators, showing lower experimental angles due to over-extrusion. (G) Bending angle comparison for 40A and 50A actuators, with simulation–experiment discrepancies attributed to Mullins effect.

sis (FEA) more closely aligned with the response of under-extruded actuators, suggesting that the over-extrusion typically employed to ensure airtightness contributes to deviations between experimental results and simulated performance.

We characterized the material-dependent mechanical response of pneumatic actuators by fabricating PneuNets via FGF using TPS pellets with Shore hardness values ranging from 6A to 50A (**Figure 4D**). Under identical input pressures, softer materials produced significantly greater deformation due to their lower elastic moduli and increased compliance. In contrast, a PneuNet printed via FFF using a commercial TPU filament (Ninjaflex Edge, 83A) exhibited minimal bending, underscoring the importance of soft materials with lower Shore hardness, readily processable through FGF, for achieving large deformations in soft pneumatic actuators.

4.2 Numerical simulation of PneuNet bending behaviors

To gain deeper insight into actuator performance and evaluate the accuracy of the simulation framework, we conducted FEA using material models calibrated from uniaxial tensile test data. For each material, we fitted a hyperelastic constitutive model and simulated the pressurization-induced deformation of PneuNet actuators. The simulated responses were then compared to experimental results to assess model fidelity.

The simulated deformation profiles closely matched the experimentally observed bending shapes, confirming that the fitted material models effectively captured the global deformation trend (**Figure 4E**). However, systematic deviations were observed in the pressure–bending angle curves across different materials.

For actuators printed with 6A, 10A, and 22A TPS pellets, experimental bending angles were consistently lower than predicted by the numerical model (**Figure 4F**). This discrepancy is likely caused by over-extrusion during printing, which increased wall thickness and overall stiffness, conditions not reflected in the idealized numerical model. In contrast, actuators printed with 40A and 50A pellets exhibited bending angles that exceeded those predicted by the numerical model (**Figure 4G**). This divergence is attributed to the Mullins effect, a stress-softening phenomenon that was not accounted for in the material models but becomes more prominent in stiffer elastomers subjected to large strains.

These comparisons emphasize the necessity of accounting for fabrication-induced variability and time-dependent viscoelastic effects to enhance the predictive fidelity of computational models for soft pneumatic actuators.

5 Demonstrations

5.1 Soft robotic hand

We designed, fabricated, and tested a fully soft robotic hand to demonstrate the ability of FGF to produce complex, integrated fluidic devices. The printing of the hand with 22A pellets took 20 hours and 40 minutes (**Movie S1**). The hand comprises five fingers, each containing three independent embedded pneumatic chambers and integrated fluidic paths (**Figure 5A**). The entire structure was printed monolithically, without any post-processing or assembly steps. We used thin outer walls (1.5 mm, three perimeters) and a 50% gyroid infill to balance compliance with airtightness (**Figure 5B**). All inflatable chambers are connected to internal channels that converge at the back of the hand within a compact routing area, allowing 15 individual tubes to supply pressurized air to each chamber for actuation (**Figure 5C**).

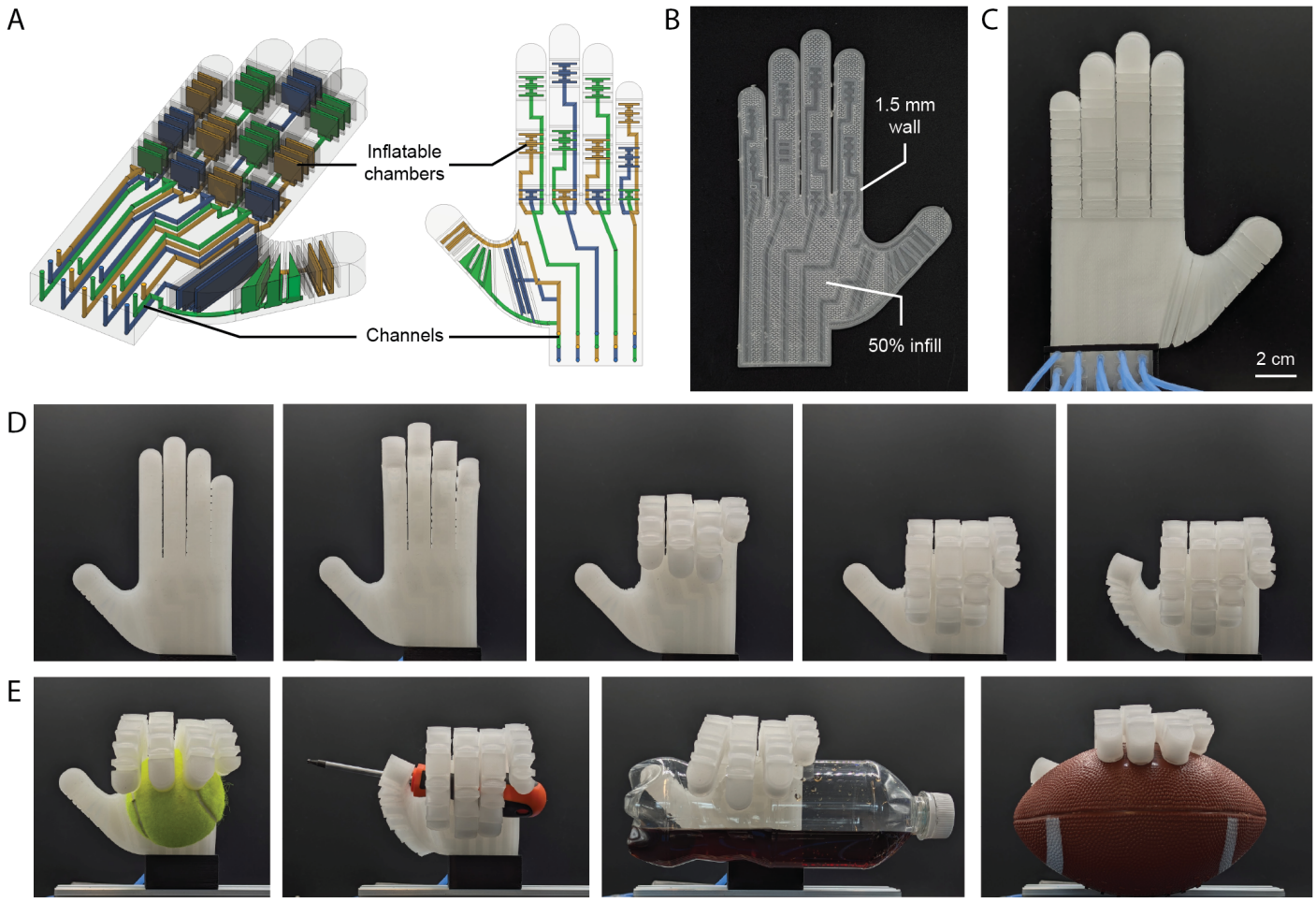

Figure 5: **Robotic hand demonstrating the reliable printing of a complex fluidic device.** (A) Semi-transparent CAD view of the hand design, with blue, yellow, and green regions indicating internal channels and inflatable chambers. (B) Close-up image of the printed hand at 3 mm height, showing thin wall structures, internal channels, and 50% gyroid infill. (C) Image of the backside of the printed hand. (D) Actuation sequence showing the robotic hand transitioning from an extended state to a fully grasping state by sequentially actuating chambers in the fingers and thumb. (E) Demonstration of the robotic hand grasping a variety of everyday objects.

Sequential actuation of the chambers enables coordinated motion across the finger segments, culminating in a full grasping configuration (**Figure 5D**). The robotic hand successfully grasps objects of varying sizes and geometries (**Figure 5E**, **Movie S2**), demonstrating the ability of FGF to produce functional soft robotic systems with complex, monolithically printed internal structures.

5.2 Soft robotic fish

We fabricated a soft robotic fish using FGF to assess the airtightness and structural integrity of monolithically printed components for underwater applications. The design was intentionally configured to demonstrate the feasibility of printing tall, complex geometries with extended bridges and overhangs, features that remain challenging for conventional FDM-based soft systems, which are typically limited to low-profile architectures. The robot consists of three sections, head, body, and tail (**Figure 6A**), and was printed using 22A TPS pellets in 18 hours and 55 minutes. The body section incorporates all pneumatic chambers, with 2 mm-thick outer walls (four printed perimeters) and unsupported bridges exceeding 10 mm in length. All three sections were printed in a single build orientation and subsequently joined using adhesive bonding (**Figure 6B**). The actuator architecture includes two independent pneumatic chambers located on the left and right sides of the body. Differential pressurization of these chambers induces lateral bending of the body and tail, generating undulatory thrust for propulsion (**Figure 6C**).

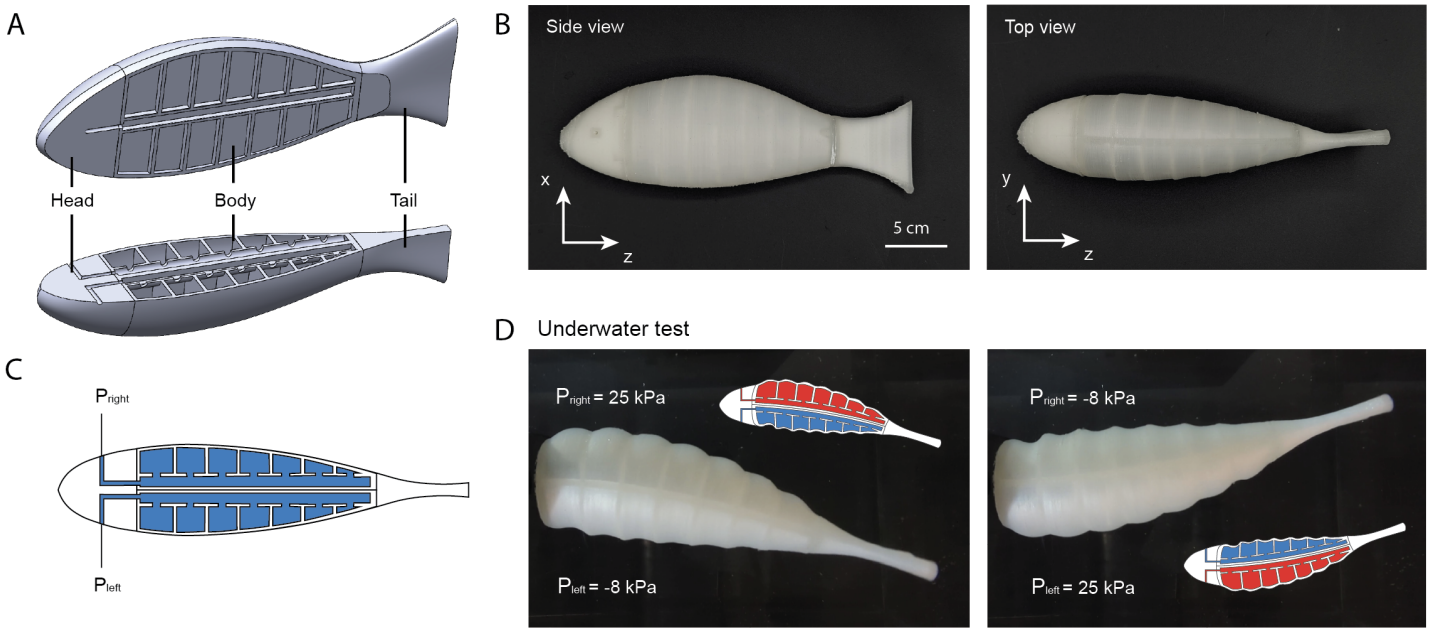

Figure 6: **Robot fish demonstrating airtight print for underwater applications.** (A) Cross-sectional CAD view of the robotic fish design, highlighting the head, body, and tail regions. (B) Photographs of the printed fish from side and top views with printing directions. (C) Schematic diagram of the actuation principle. (D) Underwater images of the actuated robotic fish, demonstrating full airtightness and functional swimming motion.

During submerged testing, the system exhibited airtight performance over repeated actuation cycles, with no detectable leakage observed (**Figure 6D**, **Movie S3**).

5.3 Wearable pressure cuff

We demonstrated the fabrication of wearable pneumatic devices by printing a soft pressure cuff with embedded inflatable chambers using 50A TPS pellets. The design incorporated a single-layer thin inner wall and a thicker outer wall, with internally connected chambers to enable uniform pressurization (**Figure 7A**). The structure was printed monolithically in 9 hours and 26 minutes. Upon inflation through a single inlet, the asymmetric wall geometry induced inward bulging of the thinner wall, generating radial compression around the limb (**Figure 7B**). The geometry was optimized to operate within standard blood pressure ranges (11.3–17.3 kPa), providing a balance between compliance and structural stiffness. Compared to the 22A pellets used in other demonstrations, the 50A material offered enhanced mechanical stability while preserving sensitivity to modest pressure changes. The cuff remained fully airtight despite its thin-wall construction, underscoring the reliability of the extrusion process. When applied to the upper arm, the cuff delivered uniform radial pressure and enabled systolic pressure measurement via an integrated pressure sensor (**Figure 7C, D**). The device maintained stable internal pressure across repeated actuation cycles, and the presence of high-frequency pressure oscillations in the recorded signal

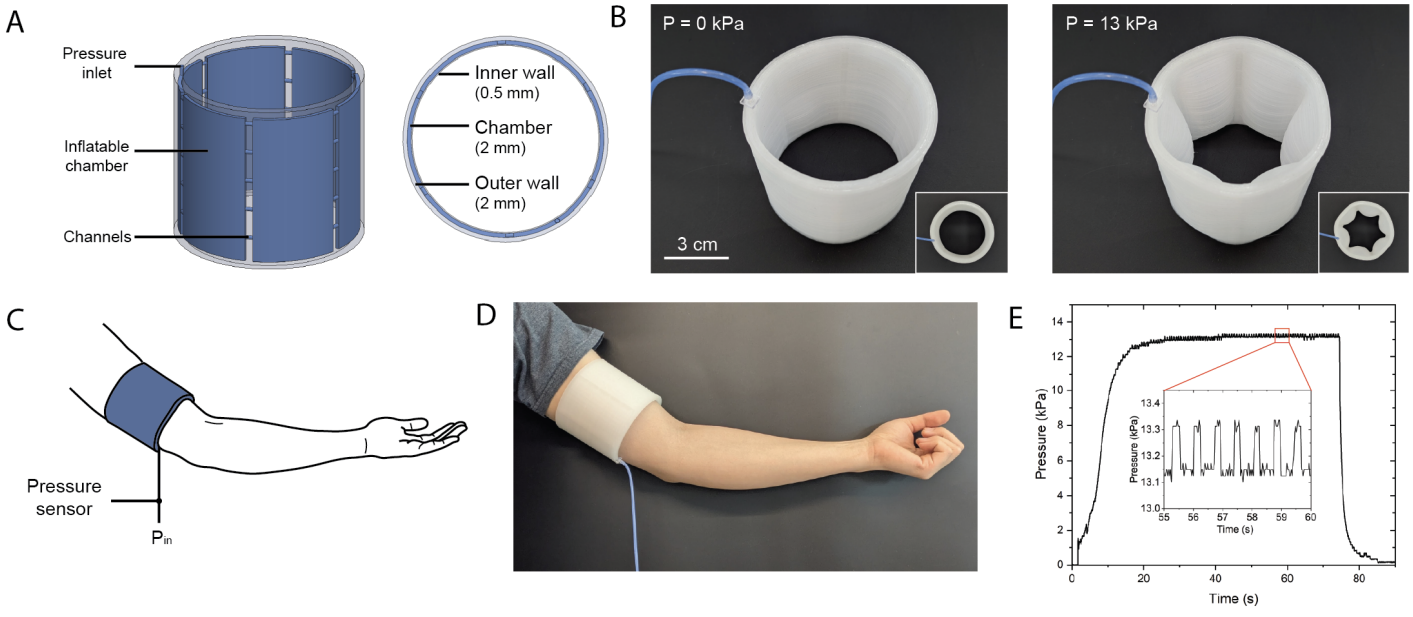

Figure 7: **Pressure cuff demonstrating wearable applications.** (A) CAD model and cross-sectional view of the pressure cuff, with blue regions showing the internal inflatable chambers and channels. (B) Photographs of the printed cuff in unpressurized (0 kPa) and pressurized (13 kPa) states, demonstrating airtight expansion. (C) Schematic diagram of the experimental setup for pressure input and sensing. (D) Demonstration of the cuff worn on the arm. (E) Pressure profile during inflation, with inset showing high-frequency pressure fluctuations from the heartbeat.

confirmed both the airtightness of the chambers and the mechanical responsiveness of the structure to dynamic loading conditions (**Figure 7E**).

6 Discussion

FGF opens the door to a vast and largely untapped library of thermoplastic materials available through the established polymer industry. This includes hydrophobic, conductive, biodegradable, and recycled materials, allowing designers to expand the functional capabilities of their 3D printed soft devices. By enabling easy access to a wide range of material properties, FGF supports application-specific customization, making it possible to tailor devices for unique performance needs at scale. This flexibility empowers new designs and use cases that go beyond what is achievable with traditional filament-based approaches. However, each new material introduces the need for dedicated investigations into its processability and the performance of the resulting printed part. This work provides a systematic framework and workflow for tuning and characterizing new materials, serving as a foundation for future exploration (**Supporting Information, Section 4**). Yet, there remains substantial potential to unlock, particularly in expanding the printable material range and pushing the boundaries of design possibilities in soft robotics.

Looking ahead, integrating multimaterial printing capabilities would enable the fabrication of complex, gradient, or functionally segmented soft robots in a single process—combining materials with the same chemistry but differing in stiffness, conductivity, or permeability within one structure. This approach can also address inherent limitations in printing overhangs and bridges by using dissolvable support materials.

In addition, closed-loop printing systems, incorporating in situ sensing and feedback control, could further enhance print reliability, improve structural integrity, and enable real-time correction of defects or parameter drifts. Together, these advancements will help transform FGF from a promising technique into a robust, versatile platform that empowers researchers, individual innovators, and startups to rapidly create novel, highly customized soft devices at scale—combining speed, material freedom, and application-specific design in ways not achievable with traditional methods.

7 Conclusion

This work establishes Fused Granulate Fabrication (FGF) as a robust and versatile fabrication strategy for both rapid prototyping and scalable manufacturing of large soft and complex devices. By enabling

the reliable extrusion of silicone-soft, airtight structures from thermoplastics with Shore hardness as low as 6A—and achieving significantly higher throughput than conventional FFF systems—FGF overcomes key limitations through coordinated material, hardware, and process optimization. We present a comprehensive testing framework that includes mechanical characterization of TPS materials, quantification of the Mullins effect, and evaluation of pneumatic actuator durability and bending performance, supported by numerical simulations. Airtightness and functional viability are demonstrated through diverse printed devices, including a soft robotic hand, an underwater fish, and a wearable pressure cuff. With access to a broad range of thermoplastic pellets, FGF offers a scalable path toward multimaterial integration, functional filler embedding, and closed-loop control, positioning it as a transformative manufacturing approach for soft robotics and next-generation flexible systems.

8 Experimental Section

Pellet printer setup: We used an Ender 3 Pro Plus FFF printer as the base platform. The standard filament print head was replaced with a pellet extruder from Direct3D. The Direct3D pellet hopper was redesigned with a steeper wall angle to enhance gravitational flow, and the internal surfaces were coated using PTFE to reduce wall friction and mitigate pellet bridging. A Raspberry Pi 4 was integrated with the system to run Klipper firmware, allowing for direct control of the printing process. Cura (5.8.1) was used for slicing.

Tensile test experiment: We fabricated all test bars according to the ASTM D412 Type C standard with a thickness of 3 mm. We printed TPE test bars using either FFF or FGF, and casted silicone test bars using FFF-printed molds. We performed tensile tests using a universal testing machine (Instron 68TM-50) with a 500 N load cell. Following the standard, we applied a strain rate of 500 mm/min during testing. For each test, we measured the initial clamp distance along with the actual width and thickness of the sample to calculate strain and cross-sectional area. We applied a prestress of 0.5 N for most test bars and used 0.1 N for materials with Shore hardness below 10A.

For the cycling tests, we programmed the Instron testing machine to pull the test bars between 0% strain and a specific maximum strain (varied across test conditions) for five cycles, followed by a final pull to a predefined maximum extension. We used a strain rate of 500 mm/min for all cycles, consistent with the uniaxial tensile tests.

PneuNet test setup: We fabricated each PneuNet using the same print parameters as those applied to

the mechanical test bars to maintain consistency across experiments. Each actuator was mounted on a fixed test frame against a black background, and images were captured at discrete pressure intervals. We quantified bending angles from these images through post-processing. For cyclic testing, we applied the same image-based analysis to the selected cycles. An Arduino Mega controlled the actuation between recorded cycles, applying 35 kPa at 5-second intervals to induce near-complete bending in each cycle.

Simulation setup: We analyzed the bending behavior of the pneumatic actuator using COMSOL Multiphysics 6.2. We conducted a 3D stationary study with a mesh defined in normal mode and element sizes ranging from 1 to 3 mm. We applied a fixed boundary condition to the surface containing the inlet connection. To account for mechanical interactions under high pressure, we defined contact pairs between adjacent chambers using a penalty factor of 1. We accounted for gravity in the vertical direction to replicate the experimental setup. To simulate internal pressurization, we applied a boundary load to the inner walls of the actuator. We quantified the bending angle by extracting the normal vector components (nx and ny) from the distal surface of the actuator.

We captured the material behavior using a third-order Ogden hyperelastic model (**Supporting Information, Section 7**). We fitted the model parameters for each material using true stress–strain data obtained from uniaxial tensile tests.

Demonstration setup: The robotic hand features 15 individually controlled pneumatic actuators. Each actuator was connected to a 12 V solenoid valve (0520F), driven by a MOSFET driver module (YYNMOS-4) and controlled via an Arduino Mega 2560. The actuators in the index, middle, ring, and pinky fingers were actuated under a uniform pressure of 90 kPa, while the thumb actuators operated at a lower pressure of 15 kPa.

The robotic fish incorporates two internal pneumatic chambers. To maximize bending, pressure was supplied to one chamber while vacuum was applied to the other. This differential actuation employed four solenoid valves, two supplying positive pressure and two supplying vacuum, to enable bending via controlled asymmetric pressurization. Positive and negative pressures were both supplied by a 12 V pump (SC3802PM-A). For underwater testing, we removed the head of the robotic fish to simplify fixture mounting and ensure stable positioning during actuation (**Movie S3)**.

In the pressure sleeve, we connected all chambers to a single pneumatic line to enable one-input control. A pressure regulator (AFR2000) was used to limit the maximum supply pressure, and airflow was modulated by selecting tubing with a narrow inner diameter of 1.5 mm. We measured internal pressure using a piezoresistive pressure sensor (XGZP6847A500KPG) connected to an analog-to-digital converter

(ADS1115).

Supporting Information

Supporting Information is available from the Wiley Online Library or from the author.

Acknowledgements

We thank Josef Neuer of Kraiburg TPE GmbH in Germany for his support in guiding the material selection process. This research was funded by the National Science Foundation (NSF) under award number 2512999.

References

[1] J. Fang, Y. Zhuang, K. Liu et al., "A Shift from Efficiency to Adaptability: Recent Progress in Biomimetic Interactive Soft Robotics in Wet Environments", *Advanced Science* **2022**, *9*, 8 2104347.

[2] M. M. Duran, G. Moro, Y. Zhang, A. Islam, "3D printing of silicone and polyurethane elastomers for medical device application: A review", *Advances in Industrial and Manufacturing Engineering* **2023**, *7* 100125.

[3] P. Polygerinos, Z. Wang, K. C. Galloway, R. J. Wood, C. J. Walsh, "Soft robotic glove for combined assistance and at-home rehabilitation", *Robotics and Autonomous Systems* **2015**, *73* 135.

[4] C. Aygül, C. Güven, S. A. Frunzi, B. J. Katz, M. P. Nemitz, "A framework for soft mechanism driven robots", *Nature Communications* **2025**, *16*, 1 1426.

[5] J. Hughes, U. Culha, F. Giardina, F. Guenther, A. Rosendo, F. Iida, "Soft Manipulators and Grippers: A Review", *Frontiers in Robotics and AI* **2016**, *3*.

[6] S. Kendre, G. Teran, L. Whiteside et al., "Printable Flexible Robots for Remote Learning", In *ASEE-NE 2022 Proceedings*. ASEE Conferences, Wentworth Institute of Technology, Massachusetts, **2022** 42267.

[7] S. Conrad, J. Teichmann, P. Auth et al., "3D-printed digital pneumatic logic for the control of soft robotic actuators", *Science Robotics* **2024**, *9*, 86 eadh4060.

[8] Y. Zhai, A. De Boer, J. Yan et al., "Desktop fabrication of monolithic soft robotic devices with embedded fluidic control circuits", *Science Robotics* **2023**, *8*, 79 eadg3792.

[9] T. J. Wallin, J. Pikul, R. F. Shepherd, "3D printing of soft robotic systems", *Nature Reviews Materials* **2018**, *3*, 6 84.

[10] H. Dong, T. Weng, K. Zheng, H. Sun, B. Chen, "Review: Application of 3D Printing Technology in Soft Robots", *3D Printing and Additive Manufacturing* **2024**, *11*, 3 954.

[11] L. Zhou, J. Fu, Y. He, "A Review of 3D Printing Technologies for Soft Polymer Materials", *Advanced Functional Materials* **2020**, *30*, 28 2000187.

[12] Y. Wu, Z. Dai, H. Liu, L. Wang, M. P. Nemitz, "Vision-based FDM Printing for Fabricating Airtight Soft Actuators", In *2024 IEEE 7th International Conference on Soft Robotics (RoboSoft)*. **2024** 249–254, ISSN: 2769-4534.

[13] Y. Wang, R. Yin, L. Jin et al., "3D-Printed Photoresponsive Liquid Crystal Elastomer Composites for Free-Form Actuation", *Advanced Functional Materials* **2023**, *33*, 4 2210614.

[14] O. D. Yirmibesoglu, J. Morrow, S. Walker et al., "Direct 3D printing of silicone elastomer soft robots and their performance comparison with molded counterparts", In *2018 IEEE International Conference on Soft Robotics (RoboSoft)*. **2018** 295–302.

[15] E. Kanhere, T. Calais, S. Jain et al., "Upgrading and extending the life cycle of soft robots with in situ free-form liquid three-dimensional printing", *Science Robotics* **2024**, *9*, 97 eadn4542.

[16] D. K. Patel, A. H. Sakhaei, M. Layani, B. Zhang, Q. Ge, S. Magdassi, "Highly Stretchable and UV Curable Elastomers for Digital Light Processing Based 3D Printing", *Advanced Materials* **2017**, *29*, 15 1606000.

[17] T. J. K. Buchner, S. Rogler, S. Weirich et al., "Vision-controlled jetting for composite systems and robots", *Nature* **2023**, *623*, 7987 522.

[18] R. MacCurdy, R. Katzschmann, Y. Kim, D. Rus, "Printable hydraulics: A method for fabricating robots by 3D co-printing solids and liquids", In *2016 IEEE International Conference on Robotics and Automation (ICRA)*. **2016** 3878–3885.

[19] G. Dämmer, S. Gablenz, A. Hildebrandt, Z. Major, "PolyJet-Printed Bellows Actuators: Design, Structural Optimization, and Experimental Investigation", *Frontiers in Robotics and AI* **2019**, *6*.

[20] J. P. Moore, C. B. Williams, "Fatigue Characterization of 3D Printed Elastomer Material", In *2012 International Solid Freeform Fabrication Symposium*. The University of Texas at Austin, **2012** .

[21] C. Tawk, R. Mutlu, G. Alici, "A 3D Printed Modular Soft Gripper Integrated With Metamaterials for Conformal Grasping", *Frontiers in Robotics and AI* **2022**, *8*.

[22] B. A. W. Keong, R. Y. C. Hua, "A Novel Fold-Based Design Approach toward Printable Soft Robotics Using Flexible 3D Printing Materials", *Advanced Materials Technologies* **2018**, *3*, 2 1700172.

[23] P. D. S. H. Gunawardane, P. Cheung, H. Zhou, G. Alici, C. W. De Silva, M. Chiao, "A Versatile 3D-Printable Soft Pneumatic Actuator Design for Multi-Functional Applications in Soft Robotics", *Soft Robotics* **2024**, *11*, 4 709.

[24] H. K. Yap, H. Y. Ng, C.-H. Yeow, "High-Force Soft Printable Pneumatics for Soft Robotic Applications", *Soft Robotics* **2016**, *3*, 3 144.

[25] J. Guo, Z. Li, J.-H. Low et al., "Kirigami-Inspired 3D Printable Soft Pneumatic Actuators with Multiple Deformation Modes for Soft Robotic Applications", *Soft Robotics* **2023**, *10*, 4 737.

[26] T. Hainsworth, L. Smith, S. Alexander, R. MacCurdy, "A Fabrication Free, 3D Printed, Multi-Material, Self-Sensing Soft Actuator", *IEEE Robotics and Automation Letters* **2020**, *5*, 3 4118.

[27] S. V. Kendre, C. Aygül, C. S. Page, L. Wang, M. P. Nemitz, "FDM-Printed CMOS Logic Gates from Flexing Beam Mechanisms for the Control of Soft Robotic Systems", *Advanced Intelligent Systems* **2025**, *7*, 2 2400468.

[28] M. Gepner, J. Mack, A. A. Stokes, "A standardized platform for translational advances in fluidic soft systems", *Device* **2025**, 100800.

[29] Y. P. Shaik, J. Schuster, A. Shaik, "A Scientific Review on Various Pellet Extruders Used in 3D Printing FDM Processes", *Open Access Library Journal* **2021**, *8*, 8 1.

[30] J. M. Justino Netto, H. T. Idogava, L. E. Frezzatto Santos, Z. d. C. Silveira, P. Romio, J. L. Alves, "Screw-assisted 3D printing with granulated materials: a systematic review", *The International Journal of Advanced Manufacturing Technology* **2021**, *115*, 9 2711.

[31] A. Georgopoulou, L. Egloff, B. Vanderborght, F. Clemens, "A Sensorized Soft Pneumatic Actuator Fabricated with Extrusion-Based Additive Manufacturing", *Actuators* **2021**, *10*, 5 102.

[32] A. Georgopoulou, S. Hamelryckx, K. Junge et al., "A multi-material robotic finger with integrated proprioceptive and tactile capabilities produced with a circular process", In *2023 IEEE International Conference on Soft Robotics (RoboSoft)*. **2023** 1–6, ISSN: 2769-4534.

[33] M. A. H. Khondoker, D. Sameoto, "Direct coupling of fixed screw extruders using flexible heated hoses for FDM printing of extremely soft thermoplastic elastomers", *Progress in Additive Manufacturing* **2019**, *4*, 3 197.

[34] L. Morita, A. Asad, X. Sun, M. Ali, D. Sameoto, "Integration of a needle valve mechanism with cura slicing software for improved retraction in pellet-based material extrusion", *Additive Manufacturing* **2024**, *82* 104045.

[35] N. Willemstein, H. van der Kooij, A. Sadeghi, "Pellet-based 3d printing of soft thermoplastic elastomeric membranes for soft robotic applications", **2025**.

Table of Contents

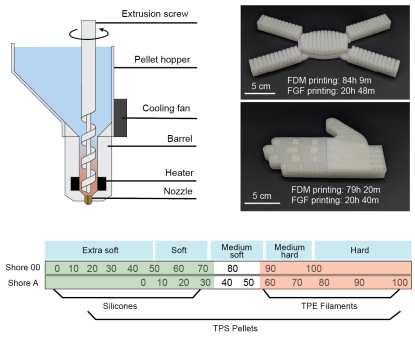

This work establishes Fused Granulate Fabrication (FGF), or pellet printing, as a robust method for fabricating air-tight, large soft devices by addressing extrusion challenges through process and material optimization. It features a case study on pneumatic actuators tested over 100,000 cycles and characterization of silicone-soft thermoplastics. Demonstrators—printed 4x faster than FFF—include a robotic hand, fish, and pressure cuff.